

# Interaction of polyomavirus internal protein VP2 with the major capsid protein VP1 and implications for participation of VP2 in viral entry

Xiaojiang S.Chen<sup>1</sup>, Thilo Stehle<sup>1,2</sup> and Stephen C.Harrison<sup>1,3</sup>

<sup>1</sup>Howard Hughes Medical Institute and Department of Molecular and Cellular Biology, Harvard University, 7 Divinity Avenue, Boston, MA 02138, USA

<sup>2</sup>Present address: Laboratory of Developmental Immunology, Massachusetts General Hospital, Boston, MA 02114-2696, USA

<sup>3</sup>Corresponding author

**A complex of the polyomavirus internal protein VP2/VP3 with the pentameric major capsid protein VP1 has been prepared by co-expression in *Escherichia coli*. A C-terminal segment of VP2/VP3 is required for tight association, and a crystal structure of this segment, complexed with a VP1 pentamer, has been determined at 2.2 Å resolution. The structure shows specific contacts between a single copy of the internal protein and a pentamer of VP1. These interactions were not detected in the previously described structure of the virion, but the location of VP2 in the recombinant complex is consistent with features in the virion electron-density map. The C-terminus of VP2/VP3 inserts in an unusual, hairpin-like manner into the axial cavity of the VP1 pentamer, where it is anchored strongly by hydrophobic interactions. The remainder of the internal protein appears to have significant flexibility. This structure restricts possible models for exposure of the internal proteins during viral entry.**

**Keywords:** non-enveloped virus/virus assembly/VP1/VP2/X-ray crystallography

## Introduction

Polyomaviruses are small, dsDNA tumor viruses. Their capsids contain 360 copies of viral protein 1 (VP1), arranged in 72 pentamers on an icosahedral lattice (Rayment *et al.*, 1982). The capsid encloses the internal proteins VP2 and VP3, as well as the viral minichromosome. The internal proteins overlap in sequence (Figure 1) and a single copy of either VP2 or VP3 associates with each VP1 pentamer (Barouch and Harrison, 1994). Crystal structures of the murine polyomavirus ('polyoma') and the closely related simian virus 40 (SV40) have revealed the architecture of the virion shell and the structure of VP1 (Liddington *et al.*, 1991; Stehle *et al.*, 1994). Long, C-terminal 'arms' of VP1 emanate from each pentamer and fold into subunits of neighboring pentamers, tying the shell together. Structures of polyoma and of recombinant VP1, complexed with various oligosaccharide receptor fragments, show how a site on the outer surface determines the specificity of initial cell attachment (Stehle *et al.*, 1994; Stehle and Harrison, 1996). After binding its recep-

tor, polyoma is believed to enter by micropinocytosis (Bolen and Consigli, 1979; Kartenbeck *et al.*, 1989), eventually reaching the nucleus. It is not known how the virus breaches the membrane barrier that separates it from the cytoplasmic or nucleoplasmic compartment. The N-terminus of VP2 is myristylated (Streuli and Griffin, 1987), and studies of myristylation-defective variants of polyoma suggest that VP2 has a role in this process (Sahli *et al.*, 1993). A variety of other non-enveloped viruses contain myristylated proteins (Chow *et al.*, 1987; Clark and Desselberger, 1988; Nibert *et al.*, 1991), and there is a link to viral entry in each case.

Low resolution (25 Å) crystallographic studies of polyoma have shown that a part of VP2/VP3 inserts into the inward-facing cavity along the 5-fold axis of a VP1 pentamer (Griffith *et al.*, 1992). *In vitro* binding studies have confirmed that the VP1 pentamer interacts tightly with VP2/VP3, and that a sequence near the common C-terminus of VP2/VP3 is necessary and sufficient for complex formation (Barouch and Harrison, 1994). In the high resolution crystal structures of SV40 (3.1 Å) and polyoma (3.65 Å), 5-fold symmetric, spike-like electron density features were seen at the top of the pentamer cavities. Thus it appears that in the virion, the VP2/VP3 polypeptide chain binds in one of five equally probable orientations to its pentameric VP1 partner. In order to understand the nature of the interactions between VP2/VP3 and VP1, we have co-expressed the VP1 with VP2/VP3 and crystallized a complex of VP1 (residues 32–316) with a VP2 fragment containing the common C-terminal 105 residues of VP2/VP3 (residues 214–318). Our structure shows that the C-terminal portion of this fragment associates with VP1 pentamer tightly and specifically through hydrophobic interactions. The larger N-terminal part of the internal protein is flexible and sensitive to gentle proteolysis.

## Results and discussion

### **Expression and characterization of complexes containing VP1 and VP2/VP3**

When expressed independently in *Escherichia coli*, VP2, VP3 and various C-terminal fragments of VP2/VP3 are insoluble. The expressed internal proteins can be purified from inclusion bodies and solubilized in 8 M urea, but efforts to refold these proteins in the presence of the relatively urea-resistant VP1 pentamers did not yield adequate amounts of soluble complex (data not shown). We therefore chose to express VP2/VP3 together with VP1. Details of the co-expression strategies are described in Materials and methods. We expressed the internal protein as a glutathione *S*-transferase (GST) fusion protein in order to facilitate purification of the complex. Introduction of a thrombin site between GST and the chosen part

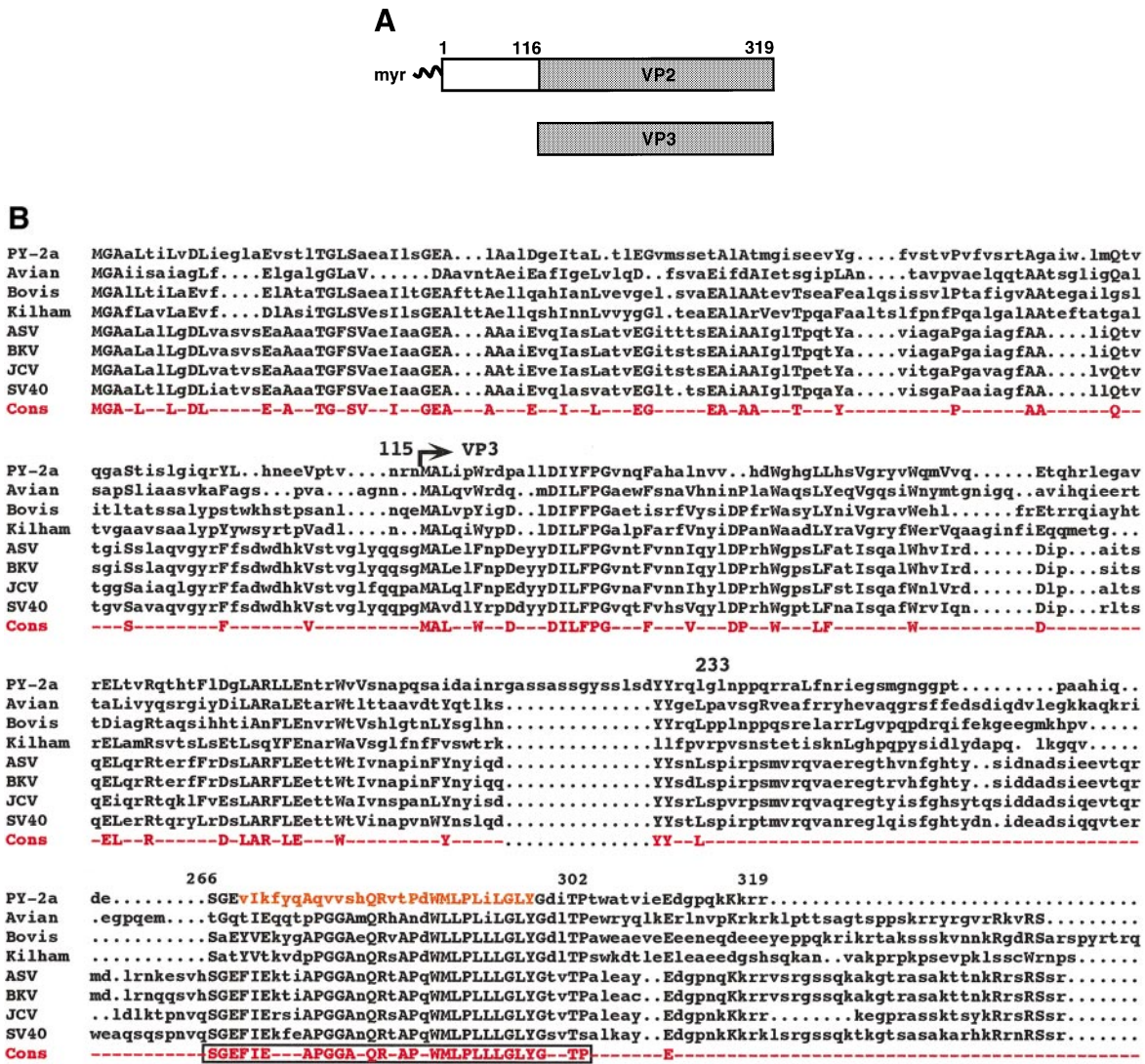


**Fig. 1.** (A) Linear alignment of polyomavirus VP2 and VP3, showing the extent of a common C-terminal segment and the N-terminal VP2-unique region. (B) Sequence alignment of VP2 in eight polyomaviruses (pileup program in GCG, Genetic Computer Group, Inc., Madison, Wisconsin). The residues are numbered according to the PY-2a strain, which is used in this work. A consensus sequence of the alignment is listed at the bottom of each line. The most conserved stretches of amino acids are boxed, and the hydrophobic helix is underlined.

of the polyoma internal protein allowed us to elute the complexes from a glutathione column by thrombin treatment. The eluted complexes were homogeneous as determined by size-exclusion chromatography (Figure 2), and the relative staining of bands (VP1:VP2 and VP1:VP3) suggested one internal protein per pentamer, consistent with earlier results from *in vitro* association of VP1 with sparingly soluble fusion proteins containing GST and C-terminal segments of VP2/VP3 (Barouch and Harrison, 1994). The stoichiometry was confirmed by quantitative N-terminal sequencing of the complexes.

To obtain evidence for a possible domain organization of VP2 or VP3, we subjected the soluble complexes to limited tryptic digestion. The internal proteins were rapidly degraded and there was no evidence for discrete smaller protease-resistant products (Figure 3A). Proteolytic treatment of dissociated virions yielded similar results (Figure 3B). Both the rapidity of the degradation and the absence of smaller species after digestion suggest that VP2 and VP3 may be relatively unfolded polypeptide chains, both

in the recombinant complexes and in those prepared from virions. These results led us to co-express shorter C-terminal fragments of VP2/VP3 with VP1 in order to obtain complexes suitable for crystallization. Plasmids encoding GST fusions with various C-terminal segments of VP2/VP3 were co-transfected into *E.coli* along with the VP1 clone (residues 32–316), and the complexes of VP1 with the various C-terminal fragments were purified from co-expressing cells as described in Materials and methods. We could only detect and purify complexes of VP1 with C-terminal fragments containing at least 45 residues of VP2/VP3, indicating a minimum requirement of VP2/VP3 sequences for VP1-association (Figure 4). The results agree with our earlier experiments using *in vitro* association (Barouch and Harrison, 1994). The complex of VP1 with the C-terminal 105 residues of VP2/VP3 (residues 214–318 of VP2) were prepared in this way, and crystals of the complex in space group P<sub>3</sub>2<sub>1</sub> (*a* = *b* = 219 Å, *c* = 99 Å) were obtained using PEG 6K as precipitant in the presence of 0.5 M ammonium

sulfate. A 2.2 Å resolution data set was collected from a selenomethionine substituted protein crystal, and a 2.65 Å resolution data set, from a native crystal (Table IA).

### Structure of the complex

The structure of this complex is shown in Figure 5; it was determined by molecular replacement using the high-

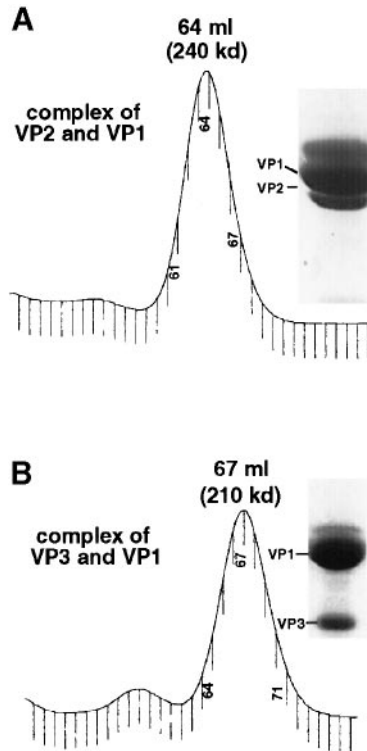


**Fig. 2.** Purification/characterization of the complexes of VP1 with VP2/VP3. The GST fusions of VP2 or VP3 associated with VP1 were cleaved from the bound glutathione resin by thrombin to elute the VP1-internal-protein complexes. The eluates were then subjected to Superdex-200 size-exclusion chromatography. The corresponding gel filtration profiles are shown in (A) and (B). Also shown beside each of the profile are SDS-polyacrylamide gel (SDS-PAGE) lanes of the pooled peak fractions.

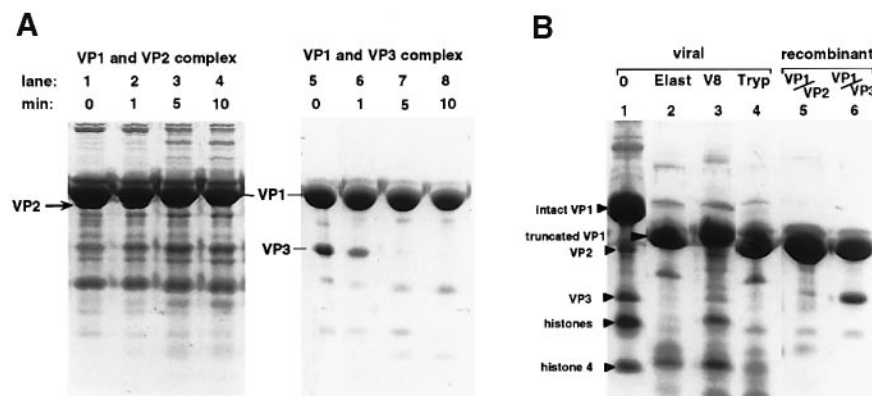


**Fig. 3.** Limited protease digestion of the complexes of VP1 with VP2/VP3. (A) SDS-PAGE (10%) analysis of the trypsin treatment of recombinant complexes of VP1 with VP2 (lane 1-4) or with VP3 (lane 5-8). VP2 and VP3 were completely digested after 5 min incubation (lane 3 and 7). A ratio of 1:1000 of trypsin to the complex (w/w) was used for the treatment at room temperature. The protease digestion was stopped at time points of 1, 5, 10 and 25 min by adding SDS-protein sample buffer to the reaction and boiling for 10 min. (B) SDS-PAGE (10%) results of elastase, V8 and trypsin treatment of the viral-derived VP1-VP2/VP3 complexes. The disassembled virus (Materials and methods) was treated with 1:1000 of trypsin (w/w, lane 4), or 1:100 of elastase (lane 2) or V8 (lane 3) for 10 min and then analyzed. The recombinant VP1-VP2/VP3 complexes were run in lanes 5 and 6 for size comparison. Lane 1 is the disassembled virus without any protease treatment, showing the position of full-length VP1, VP2, VP3 and histones from the minichromosome.

resolution model of the VP1 pentamer (Stehle and Harrison, 1997) followed by 5-fold averaging to refine initial phases. The resulting map, calculated using terms from 20–2.2 Å resolution, revealed five identical electron-density features of VP2 in the central cavity of the pentamer. The well-featured VP2 density was seen only after the 5-fold averaging (Figure 6A). This region had not been included in the 5-fold averaging, and we therefore concluded that the VP2 chain occupies five crystallographically distinct but chemically equivalent positions with respect to the VP1 pentamer with approximately equal probability, just as it does in the virion. That is, lattice contacts to the exposed part of VP2 are not sufficient to orient the 5-around-1 complex uniquely, and the ordered parts of VP2 have a relative occupancy of 20% at each of the five equivalent positions. This condition means that, after 5-fold averaging, clear electron density will be seen only for the parts of VP2 that do not overlap with their 5-fold related images. The segment of VP2 that interacts tightly with VP1 is sufficiently far from the 5-fold axis that it is clearly defined, even by the low-occupancy density (Figure 6A). Parts of VP2 close to the 5-fold axis become uninterpretable, however, because density for 5-fold related positions overlaps, especially at the top of the pentamer cavity. We are confident of the chain trace for 20 residues of VP2 and of the approximate location of eight more. Moreover, we have verified the sequence assignment using the difference map between native and selenomethionine data sets: there is a clear difference peak at Met288 of VP2. In addition, we have determined the structure of the complex in a second crystal form, which contains a shorter fragment of VP2, and obtained essentially identical results (X.S.Chen and S.C.Harrison, unpublished). Most importantly, the electron-density map for the complete polyoma particle at 3.65 Å resolution (Stehle *et al.*, 1994) shows features in its VP1 pentamer cavity that are similar to our VP2 electron density and agree well with the model for VP2 (Figure 6B). The virus map is less detailed and not as well connected, probably because it was calculated at significantly lower resolution and the diffraction data from the intact virus are less

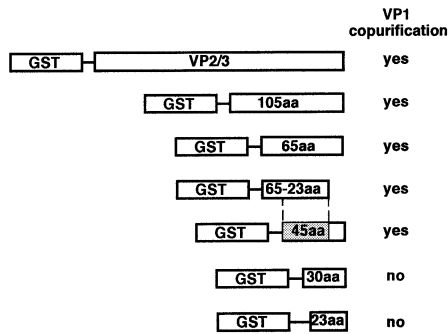


**Fig. 4.** The results of VP1 co-purification on a glutathione column with GST fusion proteins containing different C-terminal fragments of VP2. The smallest fragment capable of complexing with VP1 is the GST-C45aa of VP2.

precise. This comparison confirms that our VP2 model is directly relevant to its conformation in the virion.

Only residues 269–296 of VP2 are clearly visible in our electron-density map. These residues are located along the inner surface of a VP1 pentamer and make contact with three monomers of the pentamer (Figure 5A). They form an extended stretch, followed by a sharp 90° bend and a two-turn  $\alpha$ -helix. We do not see any interpretable electron density for residues prior to 269 or after 296, but it is clear that the VP2 chain, going from N- to C-terminus, has to enter the cavity somewhere at the base of the pentamer (Figure 5A). The five alternative locations for the polypeptide chain segment that runs from the pentamer base to the ‘top’ of the cavity probably overlap each other, blurring any electron density features from these residues. This part of VP2 may also be somewhat flexible. The chain must then loop back at the top of the cavity and run along the inner VP1 surface, forming the ordered stretch that constitutes our model (Figure 5B). The electron density for the side chains at the upper part of VP2 is ambiguous, and we cannot assign specific interactions at the top of the cavity (Figure 5A, dotted part). In contrast, there are very clear and specific interactions between the lower part of VP2 and VP1 (Figure 5C). A set of main-chain hydrogen bonds includes a short  $\beta$ -sheet-like interaction. A salt bridge/hydrogen bond network involves Asp286 of VP2 with Lys126 and Thr260 of the middle VP1 monomer (Figure 5C, green) and with Arg238 of the neighboring VP1 monomer on the right side (Figure 5C, blue). The VP2 chain executes a turn at Pro285 and leads into the extremely hydrophobic  $\alpha$ -helix. The residues on the upper side of this helix interact extensively with VP1, creating a hydrophobic interface (Figure 5C). Although these interactions seem not to involve many residues, they are able to hold together two large molecules in a highly stable and very specific manner. There is no major conformational rearrangement of the VP1 pentamer upon VP2/VP3 binding, but comparison with the uncomplexed VP1 pentamer shows that the VP2/VP3-bound pentamers of both the recombinant complexes and the virions are  $\sim 2$  Å wider at the base (Figure 5C).

The sequence alignment of VP2 from eight different polyomaviruses (Figure 1B) shows that the only long stretch of conserved amino acids is from residues 266–302 (numbered according to PY-2a), which contains the region seen in our structure (residues 269–296). Thus, the VP1–VP2 contact probably involves a similar structure in

**Table I.**

**A. Statistics for the selenomethionine and native data sets**

Data sets/Resolution (Å)	$R_{\text{sym}}$ (%) <sup>a</sup>	$\langle I \rangle / \langle \sigma \rangle$	Completeness (%)
Native: 13.0–2.60	8.7	10.4	69.7
Selenomethionine: 25.0–2.20	12.2	11.1	89.3

<sup>a</sup> $R_{\text{sym}} = \sum |I - \langle I \rangle| / \sum I$ , where  $\langle I \rangle$  is the average intensity.

**B. Refinement results**

	Selenomethionine	Native
Resolution (Å)	20.0–2.2	13.0–2.65
Number of reflections	121 606	57 822
$R_{\text{work}}$ (%) <sup>a</sup>	23.59	23.79
$R_{\text{free}}$ (%) <sup>a,b</sup>	26.53	26.46
Average B factors	22.22	23.6

<sup>a</sup> $R_{\text{work}} = \sum_{\text{hkl}} |F_{\text{cal}} - F_{\text{obs}}| / \sum_{\text{hkl}} |F_{\text{obs}}|$ , where  $F_{\text{cal}}$  and  $F_{\text{obs}}$  are the calculated and observed structure factor amplitudes.

<sup>b</sup> $R_{\text{free}}$  is the same as  $R_{\text{work}}$  except that the summation is over 5% of randomly selected reflections from the data sets, which were excluded from the refinement (Laskowski *et al.*, 1993).

all polyoma viruses. The  $\alpha$ -helical region of VP2 is especially conserved, indicating the importance of the hydrophobic interactions between the helix and VP1. The interaction centered at VP2 Asp286 and the sharp bend induced by Pro285 also appears to contribute to specificity (Figure 5B and C).

Immediately prior to the conserved region of VP2 is a stretch of about 30 residues (233–266) with poor conservation. The remaining N-terminal part (1–232) is moderately conserved. The VP2-unique region (residues 1–115) terminates in a short segment of poor conservation that links it to the beginning of VP3, suggesting a functionally bipartite organization for the first 233 residues. The highly variable region (residues 233–266) is likely to serve as a hinge, connecting the N-terminal VP2 at the base of the pentamer to the VP1-binding segment at the top. The results of gentle proteolysis (Figure 3), however, provide no evidence for distinct, tightly folded domains in VP2 in the complexes with VP1.

The last residue of our VP2 model (Tyr296) approaches the VP1 N- and C-termini at the pentamer base (Figure 5C). There is further weak electron density for VP2 beyond residue 296, running parallel to the N-terminus of VP1. The proximity of the VP1 N-terminus and VP2 C-terminus may be significant for transport of the complex to the nucleus. The nuclear localization signal (NLS) of VP1 is at its N-terminus, and the VP2 NLS is at its C-terminus (Wychowski *et al.*, 1987; Moreland and Garcea, 1991). Previous reports have shown that expression of VP1 or VP2 alone in insect cells does not lead to efficient transport to the nucleus (Montross *et al.*, 1991), while co-expression greatly increases nuclear localization of both (Delos *et al.*, 1993; Forstova *et al.*, 1993). Thus, juxtaposition of the two NLSs may enhance nuclear import of the VP1–VP2 complex. The C-terminus of VP2 also lies close to the CD loop of a VP1 subunit, where Thr114, a potential phosphorylation site (T.Benjamin, personal

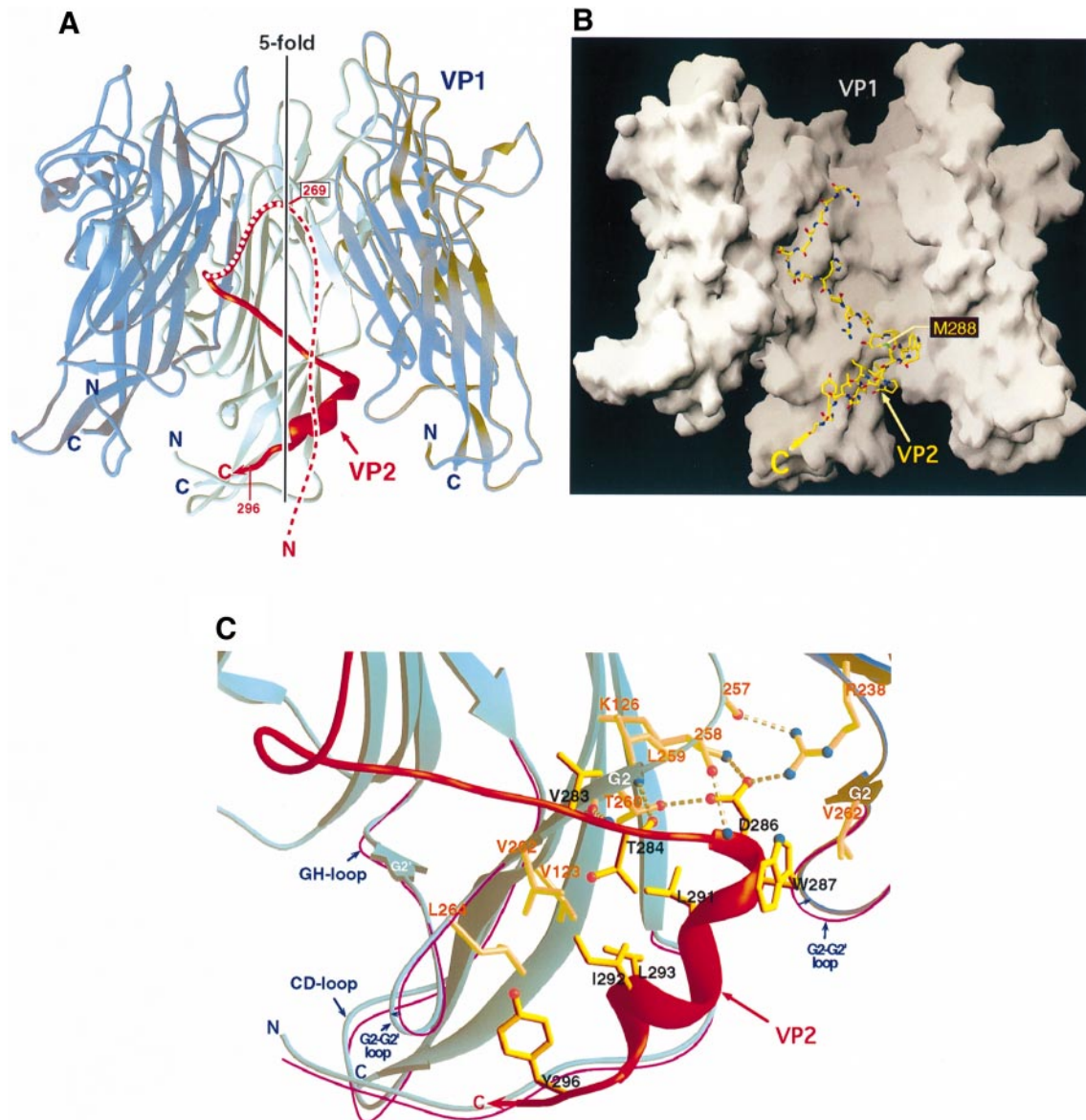


**Fig. 5.** Structure of the VP1-VP2 complex. **(A)** Cutaway view, showing VP2 in red and the three VP1 monomers that form contacts with VP2 in green (middle) and blue (left and right). The two remaining VP1 monomers that lie above the plane of the paper are not shown. Dotted line at the top of VP2 (residues Val269-Val278) indicates that the electron density in that region does not allow us to model side chains. Residues N-terminal to this dotted line of VP2 are not visible in our electron density map and are shown as dashed line. **(B)** Surface representation of the complex shown in (A). The surface of the VP1 pentamer shows various grooves, protrusions and ridges, and the VP2 chain aligns very well with these features. **(C)** Hydrophobic interactions and hydrogen bonds between VP1 and VP2. The structure of uncomplexed VP1 is shown in light colored thin lines, indicating the small structural changes that take place upon VP2 binding. The VP2 helix wedges in between the G2-G2' loops of neighboring VP1 subunits, pushing both loops slightly outwards, and the opening at the base of the pentamers is  $\sim 2$  Å wider than in uncomplexed VP1. VP2 residues are labeled in black and VP1 residues in bright orange. Parts (A) and (C) were drawn with RIBBONS (M.Carson, University of Alabama at Birmingham) and part (B) with GRASP (A.Nichols and B.Honig, Columbia University).

communication), is located. Approximately 15% of the VP1 monomers are modified (Ponder *et al.*, 1977; Bolen *et al.*, 1981; Garcea and Benjamin, 1983; Garcea *et al.*, 1985), and it is possible that VP2/VP3 has a role in selecting this threonine for modification.

#### Viral entry

If N-terminally myristylated VP2 is to have a role in membrane penetration, it must somehow become exposed or be released from the virion. The fact that the larger, N-terminal part of VP2 may be flexible and not tightly folded makes it easier for VP2 to emerge from inside the virion. Because of the very strong association of VP2

with VP1, release of the C-proximal segment of VP2 appears unlikely, unless some interaction can induce a significant conformational change in VP1. There is, in principle, a sufficient gap along the axis of a VP1 pentamer to allow an unfolded polypeptide chain to emerge. The hairpin-like conformation of VP2 seen in our structure suggests that extrusion of VP2 along the pentamer axis would require VP2 to emerge as an elongating loop, with the N-terminus last to exit and the C-terminus anchored within (Figure 7). The opening at the top of VP1 pentamer ( $\sim 12.5$  Å) may permit such a loop. It is also possible that an internal rearrangement of VP2 could allow the N-terminus to emerge first, although there is no obvious

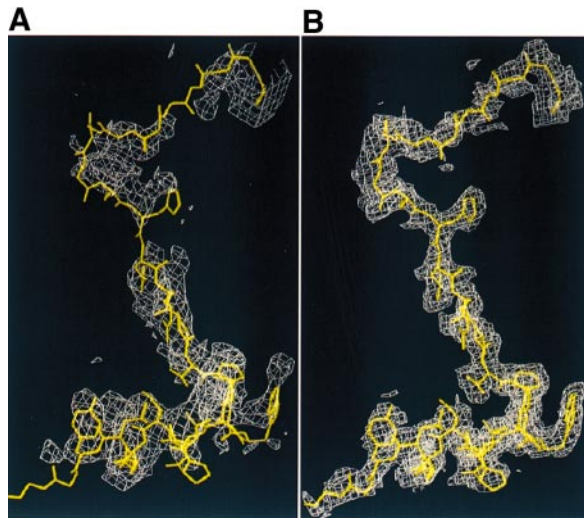


**Fig. 6.** Comparison of the final electron density map for the VP1–VP2 complex (**B**) with the map of polyomavirus at 3.65 Å (Stehle *et al.*, 1994) (**A**). The model of VP2 has been transformed into the virus map based on a superposition of the VP1 pentamers. The density for the VP1–VP2 complex is the averaged ( $2F_{\text{obs}} - F_{\text{calc}}$ ) map that was used for VP2 model building, including terms of spacings between 20 and 2.2 Å, and the density map for the virus includes terms between 12 and 3.65 Å. The density for both the VP1–VP2 complex and the virus were contoured at 1.0  $\sigma$ . Only density within 1.5 Å of the VP2 model is shown in each case. Figure prepared with program ‘O’ (A.Jones and M.Kjeldgaard, DataOno AB).

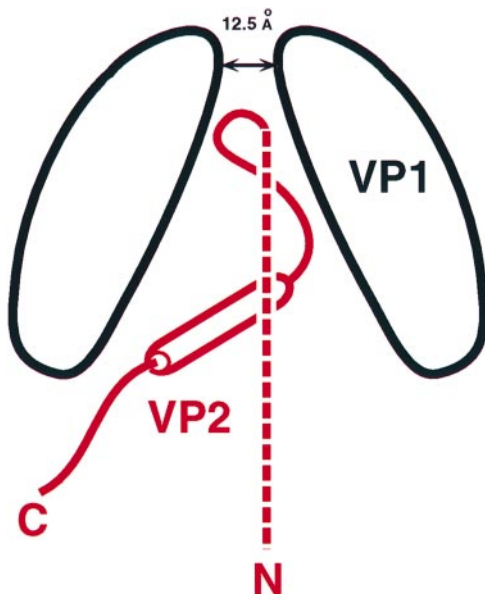


**Fig. 7.** Schematic representation of the interaction between VP1 and VP2. VP2 (red) enters VP1 pentamer (black) from the base, continuing to the upper part of the conical hollow. It then loops back to interact specifically with the inner face of VP1, forming a hairpin-like structure.

mechanism to trigger such a rearrangement. In either case, some active cellular process (e.g. one mediated by a chaperone such as Hsp70) would probably be required to withdraw VP2. A cellular protein-conducting channel has an opening of similar size (15 Å) for protein transport across the membrane of the endoplasmic reticulum (Beckmann *et al.*, 1997). Alternatively, expansion or dissociation of the virion could allow exposure of VP2

without use of the VP1 ‘pore’. In this case, we imagine that the VP1–VP2 association seen here would remain intact.

The VP1–VP2 complex resembles the AB<sub>5</sub> toxins in its 5-around-1 character (Sixma *et al.*, 1991). The virus and the toxins bind to carbohydrate receptors on the cell surface (Sixma *et al.*, 1992; Merritt *et al.*, 1994; Stehle *et al.*, 1994), and both ultimately penetrate a membrane by mechanisms not yet understood. Indeed, the carbohydrate binding sites are located at approximately similar positions with respect to the overall structure. The folds of the pentamer subunits do not, however, have any noteworthy similarities, and the insertion of the unique subunit (A or VP2) is determined by quite different sorts of contacts. The gross structural and functional parallels nonetheless suggest that the mechanism by which the AB<sub>5</sub> toxins penetrate into a cell may be relevant to the mechanism of viral entry.

## Materials and methods

### Molecular cloning

PCR was used to clone a segment encoding residues 32–316 of polyoma VP1 into the *EcoRI*–*AccI* sites of the pXp vector (Figure 8A). The encoded VP1 protein is lacking both N- and C-terminal arms (Liddington *et al.*, 1991). Similar vectors were constructed to express VP2 and VP3. For co-expression of VP1 with VP2/VP3, VP2 and VP3 (as well as truncated versions) were cloned as GST fusion proteins in the low copy number plasmid pAC (Figure 8B). *Escherichia coli* strain XA90 [*DlacproXIII*, *nalA*, *argE(am)*, *thi*, *rif<sup>r</sup>/F'laclq'ZY*, *proAB*] was used as the cloning and expressing host for all the constructs.

### Expression and isolation of the protein complex

Cells were grown in a 37°C shaker in 2× YT medium. When the OD<sub>600</sub> of the culture reached ~0.2, the temperature was lowered to 25°C, and 0.2 mM IPTG was added to induce protein expression for 15 h. Cell pellets were resuspended in buffer L (40 mM Tris–Cl pH 8.0, 0.2 M NaCl, 5% glycerol, 1 mM EDTA, 5 mM DTT) and lysed by adding 0.5 mg/ml lysozyme, 0.1% deoxycholate, 1.25 µg/ml pestatine, 2 µg/ml leupeptin and 1 mM PMSF to the cell suspension. After incubating at room temperature for about 1 h, 10 µg/ml DNase I and 5 mM MgCl<sub>2</sub> were added, and the cell lysates were then incubated at 4°C with gentle shaking until the solution was no longer viscous (4–5 h). The lysates treated by either sonication or lysozyme were centrifuged at 25 000 *g* for 1 h, and the supernatant was applied to a glutathione–Sepharose column (Pharmacia) according to the supplier’s protocol. After washing with 20× bed volume of buffer L, the proteins bound to the column were either eluted with 10 mM reduced glutathione or cleaved from the column by thrombin (Sigma, molecular biology grade). To cleave the bound proteins, ~1 NIH unit of thrombin per 100 µg protein was used to treat the resin for 2 h at room temperature. The column was then eluted with 2× bed volume of buffer L. The eluates were concentrated using Centrplus concentrators (Amicon) and further purified by Superdex-200 (Pharmacia) gel filtration chromatography. Purified VP1–VP2/VP3 complexes were directly subjected to N-terminal sequencing to determine the ratio of VP1 to VP2/VP3. For expression of selenomethionine substituted protein complexes, M9 minimal medium containing selenomethionine was used to grow the cells for protein expression.

### Virion disassembly and protease treatment

Disassembly of polyoma was carried out as previously described (Brady *et al.*, 1977). Briefly, the purified virions were treated with 10 mM DTT, 10 mM EGTA, 0.15 M NaCl and 50 mM Tris–Cl pH 8.5 for 1 h at 28°C. The disassembled virions and the recombinant VP1–VP2/VP3 complexes were treated with trypsin, chymotrypsin, V8 and elastase at room temperature. The protease digestion was stopped at different time points by adding SDS–protein sample buffer and boiling immediately for 10 min.

### Crystallography

Crystals were obtained in sitting drops in 15% PEG 6K, 0.5 M (NH<sub>4</sub>)<sub>2</sub>SO<sub>4</sub>, 10 mM DTT, 10% glycerol and 0.1 M Tris–Cl pH 8.4. The

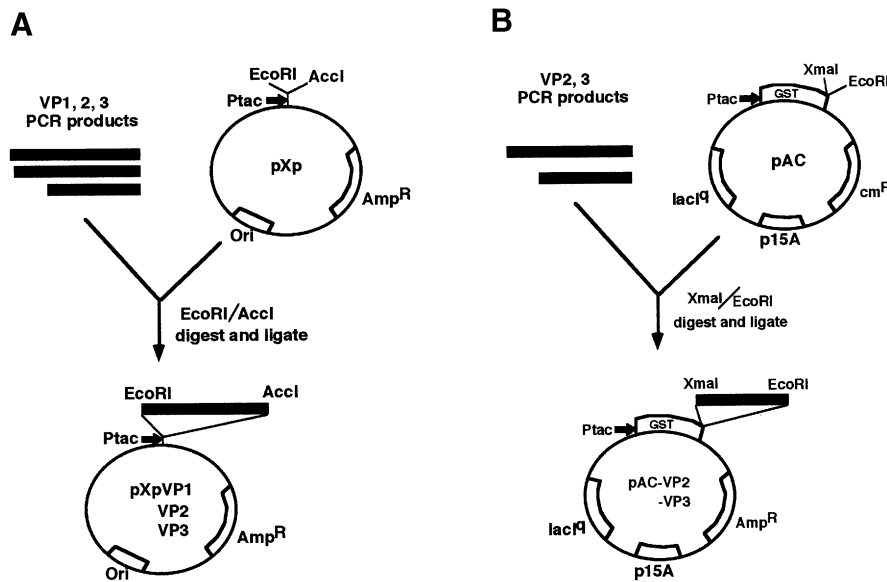


Fig. 8. Cloning strategy for VP1, VP2 and VP3 in the pXp vector (A), and for GST-VP2/VP3 and various truncations in the pAC vector (B).

space group was P3<sub>1</sub>21,  $a = b = 219 \text{ \AA}$ ,  $c = 99 \text{ \AA}$ . Data sets for both native and selenomethionine-substituted protein were collected using a CCD detector at the F1 station at CHESS and reduced using the HKL package (HKL, Inc.). Data statistics are given in Table IA. The structure was determined by molecular replacement (Navaza, 1992) using the uncomplexed free VP1 pentamer model (Stehle and Harrison, 1997). Refinement was carried out with XPLOR (Brünger, 1997) including data to 2.2 Å resolution from the selenomethionine data set. The VP1 pentamer was first refined alone ( $R_{\text{free}} = 28.0\%$ ), and after the model phases had been improved through 5-fold noncrystallographic averaging (Jones, 1992) in the absence of any VP2 residues, the model for VP2 could be built. A difference Fourier map between the native and selenomethionine data sets showed the location of VP2 Met288 and greatly facilitated model building. Five copies of VP2 per VP1 pentamer were built and refined at 20% occupancy with 5-fold non-crystallographic-symmetry constraints. The final  $R_{\text{free}}$  for the complex is 26.5% from 20–2.2 Å (Table IB).

## Acknowledgements

We thank T.Benjamin for on-going collaboration, encouragement and interest, R.Garcea for providing some of the cloning materials and support, the staff of CHESS and MacCHESS for assistance and M.Lawrence for advice and help with data collection. The work was supported in part by NIH grant CA-13202 (to S.C.H). S.C.H is an investigator in the Howard Hughes Medical Institute.

## References

- Barouch,D.H. and Harrison,S.C. (1994) Interactions among the major and minor coat proteins of polyomavirus. *J. Virol.*, **68**, 3982–3989.
- Beckmann,R., Bubech,D., Grassucci,R., Penczek,P., Verschoor,A., Blobel,G. and Frank,J. (1997) Alignment of conduits for the nascent polypeptide chain in the ribosome–Sec61 complex. *Science*, **278**, 2021–2192.
- Bolen,J.B. and Consigli,R.A. (1979) Differential adsorption of polyoma virions and capsids to mouse kidney cells and guinea pig erythrocytes. *J. Virol.*, **32**, 679–683.
- Bolen,J.B., Anders,D.G., Trempey,J. and Consigli,R.A. (1981) Differences in the subpopulation of the structural proteins of polyomavirus virion and capsids: biological functions of the multiple VP1 species. *J. Virol.*, **37**, 80–91.
- Brady,J.N., Winston,V.D. and Consigli,R.A. (1977) Dissociation of polyomavirus by the chelation of calcium ions found associated with purified virions. *J. Virol.*, **23**, 717–723.
- Brünger,A.T. (1997) X-PLOR Version 3.1: A System for Crystallography and NMTR. Yale University, New Haven, CT.
- Chow,M., Newman,J.F.E., Filman,D., Hogle,J.M., Rowlands,B.J. and

- Brown,F. (1987) Myristylation of picornavirus capsid protein VP4 and its structural significance. *Nature*, **327**, 482–486.
- Clark,B. and Desselberger,U. (1988) Myristylation of rotavirus proteins. *J. Gen. Virol.*, **69**, 2681–2686.
- Delos,S.E., Montross,L., Moreland,R.B. and Garcea,R.L. (1993) Expression of the polyomavirus VP2 and VP3 proteins in insect cells: coexpression with the major capsid protein VP1 alters VP2/3 localization. *Virology*, **194**, 393–398.
- Forstova,J., Krauzewicz,N., Wallace,S., Street,A.J., Dilworth,S.M., Beard,S. and Griffin,B.E. (1993) Cooperation of structural proteins during late events in the life cycle of polyomavirus. *J. Virol.*, **67**, 1405–1413.
- Garcea,R.L. and Benjamin,T.L. (1983) Host-range transforming gene of polyoma virus plays a role in virus assembly. *Proc. Natl Acad. Sci. USA*, **80**, 3613–3617.
- Garcea,R.L., Ballmer-Hofer,K. and Benjamin,T.L. (1985) Virion assembly defect of polyomavirus *hr-t* mutants: underphosphorylation of major capsid protein VP1 before viral encapsidation. *J. Virol.*, **54**, 311–316.
- Griffith,J.P., Griffith,D.L., Rayment,I., Murakami,T. and Caspar,D.L.D. (1992) Inside polyomavirus at 25-Å resolution. *Nature*, **355**, 652–654.
- Jones,T.A. (1992) *a, yaap,asap,@#\*??: a set of averaging programs*. In Dodson,E.J., Gover,S. and Wolf,W.(eds), *Molecular Replacement*, SERC, Daresbury, UK, pp. 91–105.
- Kartenbeck,J., Stukenbrok,H. and Helenius,A. (1989) Endocytosis of simian virus 40 into the endoplasmic reticulum. *J. Cell Biol.*, **109**, 2721–2729.
- Laskowski,R.A., MacArthur,M.W., Moss,D.S. and Thornton,J.M. (1993). PROCHECK: a program to check the stereochemical quality of protein structures. *J. Appl. Crystallogr.*, **26**, 283–291.
- Liddington,R.C., Yan,Y., Zhao,H.C., Sahli,R., Benjamin,T.L. and Harrison,S.C. (1991) Structure of simian virus 40 at 3.8 Å resolution. *Nature*, **354**, 278–284.
- Merritt,E.A., Sarfaty,S., van den Akker,F., L’Hoir,C., Martial,J.A. and Hol,W.G.J. (1994) Crystal structure of cholera toxin B-pentamer bound to receptor G<sub>M1</sub> pentasaccharide. *Protein Sci.*, **3**, 166–175.
- Montross,L., Watkins,S., Moreland,R.B., Mamon,H., Caspar,D.L.D. and Garcea,R.L. (1991) Nuclear assembly of polyomavirus capsids in insect cells expressing the major capsid protein VP1. *J. Virol.*, **65**, 4991–4998.
- Moreland,R.B. and Garcea,R.L. (1991) Characterization of a nuclear localization sequence in the polyomavirus capsid protein VP1. *Virology*, **185**, 513–518.
- Navaza,J. (1992) AMoRe: A new package for molecular replacement. In Dodson,E.J., Gover,S. and Wolf,W. (eds), *Molecular Replacement*. SERC, Daresbury, UK, pp. 87–90.
- Nibert,M.L., Schiff,L.A. and Fields,B.N. (1991) Mammalian reoviruses contain a myristylated structural protein. *J. Virol.*, **65**, 2372–2380.

- Ponder,B.A., Robinsons,A.K. and Crawford,L.V. (1977) Phosphorylation of polyoma and SV40 virus protein. *J. Gen. Virol.*, **37**, 75–83.
- Rayment,I., Baker,T.S., Caspar,D.L.D. and Murakami,W.T. (1982) Polyoma virus capsid structure at 22.5 Å resolution. *Nature*, **295**, 110–115.
- Sahli,R., Freund,R., Dubensky,T., Garcea,R., Bronson,R. and Benjamin,T. (1993) Defect in entry and altered pathogenicity of a polyoma virus mutant blocked in VP2 myristylation. *Virology*, **192**, 142–153.
- Sixma,T.K., Pronk,S.E., Kalk,K.H., Wartna,E.S., van Zanten,B.A.M., Witholt,B. and Hol,W.G.J. (1991) Crystal structure of a cholera toxin-related heat-labile enterotoxin from *E.coli*. *Nature*, **351**, 371–377.
- Sixma,T.K., Pronk,S.E., Kalk,K.H., Wartna,E.S., van Zanten,B.A.M., Berghuis,A.M. and Hol,W.G.J. (1992) Lactose binding to heat-labile enterotoxin revealed by X-ray crystallography. *Nature*, **355**, 561–564.
- Stehle,T. and Harrison,S.C. (1996) Crystal structures of murine polyomavirus in complex with straight-chain and branched-chain sialyloligosaccharide receptor fragments. *Structure*, **4**, 183–194.
- Stehle,T. and Harrison,S.C. (1997) High-resolution structure of a polyomavirus VP1-oligosaccharide complex: implications for assembly and receptor binding. *EMBO J.*, **16**, 5139–5148.
- Stehle,T., Yan,Y., Benjamin,T.L. and Harrison,S.C. (1994) Structure of murine polyomavirus complexed with an oligosaccharide receptor fragment. *Nature*, **369**, 160–163.
- Streuli,C.H. and Griffin,B. (1987) Myristic acid is coupled to a structural protein of polyoma virus and SV40. *Nature*, **326**, 619–622.
- Wychowski,C., Benichou,D. and Girard,M. (1987) The intra-nuclear location of simian virus 40 polypeptides VP2 and VP3 depends on a specific amino acid sequence. *J. Virol.*, **61**, 3862–3869.

*Received January 19, 1998; revised and accepted April 3, 1998*